

Citation for published version:
Ibrahim, YI, Kershaw, T & Shepherd, P 2020, 'Improvement of the Ladybug-tools microclimate workflow: A verification study', Paper presented at IBPSA-England Building Simulation and Optimisation Conference 2020, Loughborough , UK United Kingdom, 21/09/20 - 22/09/20.

Publication date: 2020

Document Version Publisher's PDF, also known as Version of record

Link to publication

Publisher Rights Unspecified

University of Bath

Alternative formats

If you require this document in an alternative format, please contact: openaccess@bath.ac.uk

General rights

Copyright and moral rights for the publications made accessible in the public portal are retained by the authors and/or other copyright owners and it is a condition of accessing publications that users recognise and abide by the legal requirements associated with these rights.

If you believe that this document breaches copyright please contact us providing details, and we will remove access to the work immediately and investigate your claim.

Download date: 09 Mar 2023

Improvement of the Ladybug-tools microclimate workflow: A verification study

Yasser Ibrahim¹, Tristan Kershaw¹, Paul Shepherd¹ Department of Architecture & Civil Engineering, University of Bath, Bath, UK

Abstract

Over the past two decades, there has been a marked increase in the consideration of outdoor thermal comfort by urban planners. Several researchers have developed their own models for a better understanding of the human energy exchange with their surrounding environment. Among those models developed is the Ladybug-tools microclimate model, the plugins of Grasshopper3D. These parametric design tools are acknowledged for being time and resource efficient.

In this paper, modifications to the Python source code, in terms of ground reflectivity, radiative heat transfer coefficient, projected area factor and reflected radiation were made to improve the accuracy of the model. The modified model's accuracy is verified against the validated software, ENVI-met V.4.4.4. A hypothetical simple urban geometry was simulated within each model. The analyses of the thermal performance are presented for two different locations, representing hot arid and temperate climates, namely Cairo, Egypt, and London, UK, for extreme summer and winter conditions. Results are presented in terms of the Mean Radiant Temperature (MRT) and the Universal Thermal Climate Index (UTCI). Results show a good level of conformity between the models particularly in terms of the UTCI, $R^2 = 0.98$.

This study aims to present a more precise modelling methodology for the outdoor microclimate. The modified model allows for a better parameterisation of the outdoor environment and can be considered as rigorous for modelling the outdoor conditions as fully integrated engines, albeit in a significantly less time, allowing parametric optimisation of urban geometries to become a viable proposition.

Introduction

During the last century, human thermal perception and comfort have always been a degree to be assessed, a boundary to be defined and a satisfaction to be quantified. Due to the increasing knowledge about the human energy exchange and the non-stopping developments onto the computational power, the last four decades have been witnesses for the development of thermal comfort indices and also a remarkable number of computational models to quantify the thermal comfort or the constituents thereof. Examples of these models are abundant, for instance but not limited to, ENVI-met (Bruse, 2020), RayMan (Matzarakis, et al., 2007), SOLWEIG (Lindberg, et al.,

2016), CityComfort+ (Huang, et al., 2014), CitySim Pro (Robinson, et al., 2009), Rakha's Model (Rakha, et al., 2017) and the Microclimate Model by Mackey, known as the Ladybug-tools Model (Mackey, et al., 2017). Among these models, as compared to field measurements (Elnabawi, et al., 2013, Yang, et al., 2013, Forouzandeh, 2018), ENVI-met has long been used in various studies (Sharmin, et al., 2017, Santamouris, et al., 2018) as one of the most accurate models to simulate the outdoor microclimate. However, the excessive simulation time the model requires is of the main drawbacks of ENVI-met. The Ladybug-tools model, on the other hand, harnesses the parametric capabilities of Grasshopper for Rhino3D (McNeel, 2020) to manipulate multiple design parameters and iterate different geometry configurations. The model simplifies the long-wave radiation flux from the vegetation, yet can simulate the outdoor microclimate in a considerably less time relative to the other models, especially CFD-based models such as ENVI-met.

This feature allows the Ladybug-tools model to simulate as many geometry configurations as the designer reckons to be crucial for assessment on a year-round temporal basis as opposed to other studies which ostensibly optimises the urban canyon geometries, yet intrinsically are limited to a few number of canyon configurations (Allegrini, et al., 2015, Jamei and Rajagopalan, 2019). Based on previous studies using the same model (Naboni, et al., 2017, Naboni, et al., 2018), we sought to understand how the model estimates the Mean Radiant Temperature (MRT) as one of the main constituents of outdoor thermal comfort represented by the Universal Thermal Climate Index (UTCI).

This paper presents the modifications made to the Python source code used to calculate the *MRT* and the resultant *UTCI*. Thereafter, the paper shows the model's responsiveness to the different thermal conditions within a street canyon by comparing the modified model's results to the validated software, ENVI-met V.4.4.4.

Methodology

Methods

Ladybug-tools model

Within the model, where the outdoor conditions are being included, the *MRT* is calculated as the sum of the three components; the long-wave radiation from the surrounding surfaces; the amount of the sky long-wave radiation absorbed by the human body; and the additional

amount of absorbed solar short-wave radiation. The longwave radiation from surfaces is estimated by using the following formula:

$$MRT_{Surface} = \left[\frac{\sum_{i=1}^{N} (T_s^4 \cdot F_s + T_e^4 \cdot F_{ns})}{\sum_{i=1}^{N} F_s} \right]^{1/4}$$
 (1)

Where T_s is the outside surface temperature calculated by virtue of EnergyPlus. T_e is the ambient temperature of one surface and is assumed to be equal to the ambient air temperature as shaped by the surrounding surfaces. F_s is the view factor between the point of interest and a specific surface and F_{ns} is the non-surface view factor, i.e. view factor to surfaces other than that specific surface. Angle factors are calculated by tracing back the number of spherical vectors hitting one surface and dividing that number by the total number of vectors emanating from each point. In the same context, the EnergyPlus solar distribution module "Full Exterior with Reflections" is used to account for the direct and sky solar radiation diffusely reflected by the ground and the surrounding surfaces in addition to the shadowing therein. A number of receiving points proportional to the size of the surface are allocated and, using the same ray-tracing method mentioned above (90 rays for each receiving point), view factors are calculated and the factor of reflected radiation is estimated accordingly (DoE, 2019: Section 6).

The absorbed sky long-wave radiation is calculated by following the formula specified within the MENEX model (Blazejczyk, 2005) as follows:

$$MRT_{sky} = f_{svv} \cdot \left(\frac{L_a}{\alpha_{lw} \cdot \sigma}\right)^{1/4} - 273.15 \tag{2}$$

Where f_{svv} is the sky view from a certain point unobstructed by opaque surfaces. L_a is the terrestrial sky long-wave radiation, and is obtained from the .epw file. α_{lw} is the emissivity of the human body for long-wave radiation (default value of 0.95), and σ is the Stephan Boltzmann constant $(5.667 \cdot 10^{-8} \ W/m^2 K^4)$. As for the short-wave solar radiation, the model accounts for the absorbed portion by means of the effective radiant field (ERF) specified within the SolarCal model (Arens, *et al.*, 2015) and the normative appendix (C) of (ASHRAE, 2017a) in terms of the three components; the direct; diffused; and reflected solar radiation, where the latter is defined with reference to the global horizontal radiation as follows:

$$ERF_{solar} = \frac{\alpha_{sw}}{\alpha_{lw}} \cdot \left[\left(0.5 \cdot f_{eff} \cdot f_{svv} \right) \left(I_{Global} \cdot R_{floor} + I_{diff} \right) + \left(f_{p} \cdot f_{eff} \cdot I_{Dir} \right) \right]$$
(3)

Where α_{sw} is the absorption coefficient for the short-wave radiation (default value of 0.7), f_{eff} is the fraction of the body exposed to radiation (0.696 and 0.725 for a seated and a standing person respectively). I_{Global} , I_{diff} , I_{Dir} are the global, diffused and direct normal radiation respectively. R_{floor} is the floor/ground reflectivity and f_p is the projected area factor and is derived from the projected area A_p , which values in turn were empirically

obtained with reference to the solar altitude and azimuth as in (Fanger, 1972) and (ASHRAE, 2017a). The amount of additional MRT due to solar radiation is eventually calculated in terms of ERF, f_{eff} , and the radiative heat transfer coefficient (h_r) as follows:

$$MRT_{sol} = \frac{ERF_{solar}}{f_{off}} \cdot h_r$$
 (4)

ENVI-met

The CFD numerical model ENVI-met is one of the most accurate models for assessing the outdoor thermal comfort, despite some limitations that could entail deviations from field measurements (Sharmin, et al., 2017). The model accounts for all the heat exchange processes between the human body represented in a cyliderical shape and the surrounding surfaces, vegetation (soil-plant cycle) and the airflow field in high spatiotemporal resolutions. In addition, a full range of thermal comfort indices, e.g. *UTCI* and the physiological equivalent temperature (*PET*) are available, albeit using a paid-for license. ENVI-met calculates the *MRT* following the formula:

$$MRT = \left\langle \frac{1}{\sigma} \left(Q_{lw} + \frac{\alpha_{sw}}{\alpha_{lw}} \cdot \left(Q_{diff} + Q_{dir} \right) \right) \right\rangle^{1/4}$$
 (5)

The reflected radiation is accounted for within the direct radiation component Q_{dir} , while Q_{diff} is the incoming diffused solar radiation, whereas the incoming long-wave radiation, Q_{lw} is partitioned into two equal portions, one of which is shared by the ground, while the other is shared by the sky, vegetation and building surfaces as follows:

$$Q_{lw} = 0.5 \cdot \left(F_{v} \cdot \overline{\varepsilon_{v}} \cdot \sigma \cdot \overline{T_{v}}^{4} + F_{s} \cdot \overline{\varepsilon_{s}} \cdot \sigma \cdot \overline{T_{s}}^{4} + f_{svv} \cdot Q_{lw_{s}} \right) + 0.5 \cdot \left(\varepsilon_{g} \cdot \sigma \cdot T_{g}^{4} \right)$$

$$(6)$$

where F_v is the view factor to the tree, $\overline{\varepsilon_v}$ and $\overline{\varepsilon_s}$ are the average emissivity of all trees and surfaces respectively. $\overline{T_v}$ and $\overline{T_s}$ are the average temperature of all the trees' leaves and the surfaces respectively. Q_{lw_s} is the downward sky long-wave radiation and is equal to L_a when "forcing radiation" is used. ε_g and T_g are the ground's respective emissivity and temperature. See (Huttner, 2012) for the detailed calculation for each of these components.

Model modifications

Examination of the Python code at each step of the MRT calculation has revealed a number of inaccuracies. First, the clothing absorptivity which might be input by the user within the "Comfort Recipe" component, to replace the α_{sw} is fixed to 0.7, no matter the input value. Also, the floor reflectivity of the outdoor surfaces is fixed within the "View Factor Calculator" component as a default value of 0.2. We redefined the absorptivity to allow the user to change the absorptivity and also developed a new piece of code to allow the user to change the reflectivity. In this study, floor reflectivity was set to 0.3 as an average between the walls and ground albedo. Second, the

radiative heat transfer coefficient, h_r was assigned the same value for both indoor and outdoor calculations as 6.012. We redefined the variable conditionally to be 4.7 for indoor calculations as recommended by the ASHRAE handbook of fundamentals (ASHRAE, 2017b), and 6.0 for outdoor calculations as defined in a JavaScript within the ASHRAE 55-2017, Normative Appendix "C" (ASHRAE, 2017a). Thirdly, since the standing position is more common for outdoor microclimate simulations, the effective fraction of the body, $f_{\it eff}$ and the projected area factor, f_p were set to represent a standing person (f_{eff} = 0.725 and f_p derived from the "SplineStand" function in the Ladybug legacy component) instead of a sedentary position. Fourthly, the MRT values were multiplied by their inverted sky view factor (surface view factor) during the night hours since they were merely accounting for the sunlit hours. Moreover, based on Arens, et al. (2015), the SolarCal model postulates that the reductions in diffuse radiation due to protruding surfaces are compensated by the reflected radiation and vice versa. As mentioned earlier, the reflected radiation was defined in terms of the global horizontal radiation, and hence, within the Ladybug-tools model, it is assumed that I_{Global} is confined to I_{diff} in case of solar beam obstruction. The assumption is fairly accurate within internal environments where the amount of radiation received is limited to that coming from the window aperture. However, within the external environment, an organism will receive an additional amount of direct normal radiation, reflected by the urban surfaces. Consequently, the reflected radiation (I_{ref}) was redefined in terms of I_{Dir} following (ASHRAE, 2017a)

$$I_{ref} = 0.5 \cdot f_{eff} \cdot (1 - f_{svv}) \cdot I_{dir} \cdot R_{floor}$$
 (7)

The reflectance of diffused radiation was not considered since it requires extensive scripting which is not addressed in this study. Finally, the Solar Time function was activated within the Ladybug legacy component in order for the solar altitude (defining sunlit hours) to match those within the .epw file.

Simulation setup

Modelling and parameterisation

A hypothetical geometry layout is presented in this paper to allow for a comprehensive analysis of each model's performance at different scenarios of solar exposure. As shown in Figure 1, the layout was modelled in both ENVImet and Ladybug-tools on a grid size of 2m assuming no vegetation or building fenestrations. Default construction materials were used form the ENVI-met database and their thermal properties were fed into the EnergyPlus simulations. Unknown properties were obtained from Engineering-Toolbox (Engineering-ToolBox, Ground temperatures were obtained from the .epw file (Table 1). Initial indoor temperature was set in ENVI-met to 20°C. Also, internal gains and equipement loads in Ladybug-tools were set to zero with no artificial heating or cooling loads, since ENVI-met assumes no internal loads. Throughout EnergyPlus setup in Ladybug, TARP and DoE-2 algorithms were used as the inside and outside convective heat transfer modules respectively. On the other hand, the Conduction Transfer Function (CTF) module was used since it requires further interventions within the code to change the conduction algorithm.

Table 1: Input parameters for both models

Parameter	Thermal properties				
Material	Roofs	Walls	Ground	Unit	
Reflectivity	0.50	0.40	0.05	Decimal	
Absorptance	0.90	0.90	0.98	Decimal	
Density	1900	1500	1280	kg/m ³	
Specific Heat	800	650	945	J/kg·K	
Conductivity	0.84	0.44	1.8	W/m·K	
Roughness	Rough	Rough	Rough	-	
Parameter	Soil temperature				
Scenario	7 th Jun	17 th Jan	28th Jun	1st Feb	
Temperature	25°C	15°C	11°C	7°C	

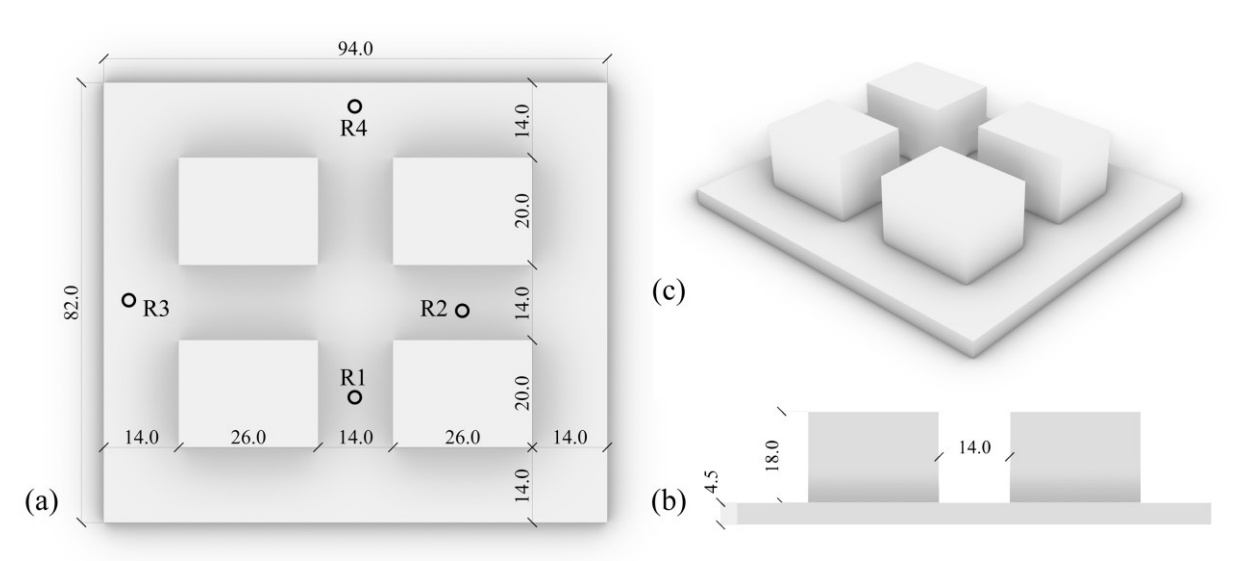


Figure 1: Model geometry and receptors of interest (a) top view (b) side view, and (c) 3D view (Dimensions in metres).

Simulation scenarios

In this study, the models' performances in different climatic regions are analysed based on two different locations, namely Cairo, Egypt as a representation for a hot-arid climate, and London, UK for a temperate climate. The weather files for both cities were obtained from (DoE, 2020), thereafter used as the boundary conditions for each model (using the full-forcing option in case of ENVImet). Simulations were run for a 24-hour period on the external hot and cold days within the .epw files; 7th June and 17th January in Cairo; and 19th August and 14th February in London. It is worth mentioning that ENVImet simulations were run using a student license which does not allow parallel core computing.

Results and discussion

Summer MRT

As for Cairo, the modifications appear to be effective within north-south (N-S) canyons as in R1, in other words where the solar radiation is blocked most of the day except for around the noon hours (11am-1pm) in addition to the points outside the canyon (R3 and R4). As shown in Figure 2, within R1, the new model resembles ENVI-met (EM) values particularly during the hours 8-10am and 2-4pm due to the amount of reflected radiation it receives. Having EM as the benchmark, MRT difference, (ΔMRT) between the new (LB-N) and the original model (LB-O) has reached its maximum at 2pm as 14.8°C. At 12pm, EM and LB-N decline due to the high solar altitude and hence reduced long-wave radiation are received from surfaces, however the declination is steeper in LB-N most probably owing to the low projected area factor (f_p) of the human body whereas in EM the human body is represented by a cylindrical shape. Moreover, modifications to the longwave radiation received during the night hours are not as clear as they are in the points outside the canyon as in R3, where the points have less surface view factor. Having the notion that EM averages the long-wave radiation from all the surfaces within a layout so as to reduce the calculation time, and the notion that EM was reported to underestimate the MRT during the night hours (Huttner, 2012, Forouzandeh, 2018), it could be claimed that LB-N might possibly be more accurate if compared to field measurements. ΔMRT in R3 is highest at 12pm of 11.4°C where LB-O receives large amount of global horizontal radiation (I_{Global}) associated with the solar altitude of the succeeding hour and its corresponding higher projected area factor.

In London, where the highest solar altitude in August is $\sim 51^\circ$, east-west (E-W) canyons as in R2 remain shaded for most of the day. This is clear where EM and LB-N maintain higher MRT values during the hours 9am-5pm with maximum ΔMRT at 3pm of 13.2°C. Night-time differences are slightly larger than Cairo since the sky downward long-wave radiation in EM is calculated based on the air temperature (which is lower in London), and the atmospheric water vapor, whereas in LB-N is simplified

and calculated in terms of the terrestrial sky long-wave radiation (almost similar to Cairo). Another potential reason is the heat storage within the surfaces which is accounted for in EM as opposed to LB (EnergyPlus) which takes no account of the heat storage in its surface energy balance when using the Conduction Transfer Function algorithm, as used in this study (DoE, 2019).

Similar to Cairo, weighting the surfaces' long-wave radiation by their view factors is more potent within the points outside the canyon. Maximum ΔMRT at R4 is noticed at 2pm as 9.24°C. On the other hand, LB-N has overestimated the MRT during 9am-12pm, however maintained less deviation at 1pm-3pm. This could be ascribed to the relatively higher f_p of a standing person compared to a seated one due to self shading in case of the latter during the hours (9am-11pm). Also, while the highest solar altitude is incident at 1pm, LB-O shows a leap due to not considering the solar time.

Winter MRT

In Cairo, the modifications appear to be almost uniform throughout the whole layout. The effect is clearly perceptible during the sunlit hours due to the differences between the global and direct radiation, which range between (42-342 W/m²) and (6-92 W/m²) for I_{Global} and I_{dir} respectively. Hence, the reflected radiation is diminished regardless the other factors, f_p and f_{eff} . It's worth mentioning that the MRT is calculated for the daytime and night-time separately in LB. That explains the LB-O falls at sunrise (7am) and leaps at sunset (6pm) which are clearer in R4, and which are dampened in LB-N. The greatest ΔMRT was registered during the hours 6pm-12am as on average 2.4°C and 6.1°C in R2 and R4 respectively. Maximum differences during sunlit hours were registered at 1pm as 1.5°C for R2 and at 11am as 4.4°C for R4.

Peculiarly, in London, although the day of simulation is overcast, direct normal radiation values are higher than those of the global and the diffused radiation which range between (222-337 W/m²) and (32-239 W/m²) for I_{dir} and both I_{Global} and I_{diff} respectively. Having the notion that the highest solar altitude on Feb 14th is ~25°, both R1 and R3 remain shaded from the sunrise until 11am. This explains the higher MRT values the LB-N possesses during these hours while being calculated with reference to the higher I_{dir} values as opposed to the LB-O which values are estimated with regards to the lower I_{diff} values. Apart from these outliers, LB-N maintains a reasonable trend compared to that of EM. It's worth noting that the inside surface temperatures, as calculated by EnergyPlus, have an average of 6°C, a share of which is conducted to the outside face, keeping the outside surface temperatures at an average of 2°C. A slight increase ensue owing to the ambient air temperature. This clarifies the relatively higher deviations during the night hours where EM surfaces absorb rather than emit the heat to the outdoor spaces, keeping the MRT values at an average of -6.5°C.



Figure 2: MRT results at different receptors for the four scenarios

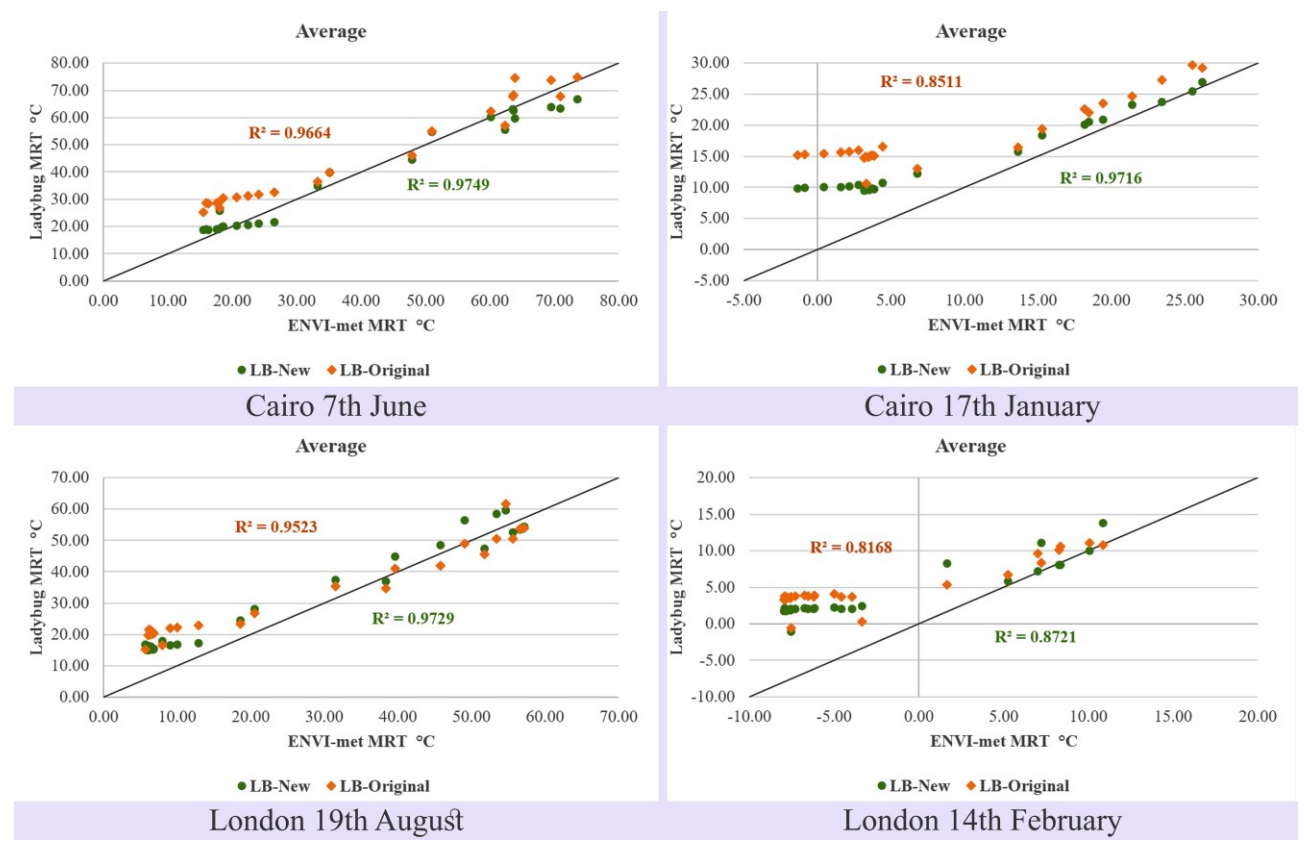


Figure 3: Scattered plots for the average MRT values over the whole layout within the four scenarios.

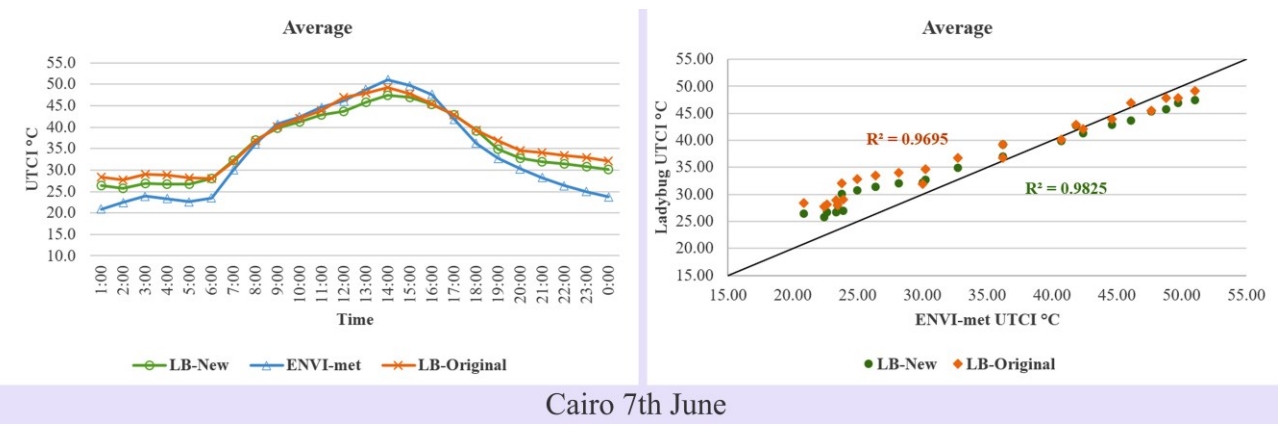


Figure 4: Average UTCI for Cairo on 7th June.

Average MRT

Figure 3 shows the MRT distribution for the average values over the whole layout. LB-N appears to show better performance in all scenarios, with greater improvements in winter both in Cairo and London. It can be noticed that, within Cairo 7^{th} June, redefining the reflected radiation with reference to the direct normal radiation (daytime hours) have shown the greatest improvement, whereas within the other scenarios weighting the surfaces' long-wave radiation by their view factors (night-time hours) was the most effective. Maximum ΔMRT was registered at 12pm in Cairo 7^{th} June as 6.7° C while 5.6° C, 5.8° C and 1.8° C were registered during the hours 6pm-12am for London 19^{th} August, Cairo 17^{th} January and London 14^{th} February respectively. Both models' correlations with EM along with the error

calculations represented by the root mean squared error (RMSE) are showed in Error! Not a valid bookmark self-reference..

Table 2: Root mean squared error and coefficient of determination between the ladybug original and new models and ENVI-met.

	RMSE		R^2	
	LB-N	LB-O	LB-N	LB-O
7 th Jun	3.9	7.9	0.974	0.966
19th Aug	6.9	9.1	0.973	0.952
17 th Jan	6.1	10.1	0.972	0.851
14th Feb	7.1	8.2	0.872	0.816

Average UTCI

Influenced by the radiant temperature results, the UTCI values are seen to be improved relative to the respective newly estimated MRT. Figure 4 is an example of the average UTCI values over the layout in Cairo on 7^{th} June. The modifications are clearer during the night hours with a maximum UTCI difference at 4am as $2.1^{\circ}C$. During the daytime, although the LB-N shows lower values than both LB-O and EM, the general trend resembles that of EM. RMSE was lowered from 4.44 to 3.45 with a stronger correlation, R^2 of 0.982 as compared to 0.969 for LB-O.

Conclusion

This paper presented a methodology for improving the Ladybug-tools workflow in modelling the outdoor microclimate. On average, it took 5 minutes to simulate each of the scenarios using The Ladybug-tools model as compared to 21 hours using ENVI-met which might approximate 3 hours if parallel core simulation is used, however, a far more expensive license is required. This qualifies the Ladybug-tools model to be top of the list of the microclimate models when it comes to optimisation studies, where simulating an urban canyon year-round or simulating hundreds of geometry configurations becomes viable. The modifications presented in this study aimed to gauge the responsiveness of the modified Ladybug-tools model to the different climatic conditions within various points of interest whether inside or outside the canyon they were. Throughout the verification of the new model's results as compared to ENVI-met results, the following insights can be drawn.

Variations in the models' surface energy balance calculation had to be taken into consideration. The threenode model used in ENVI-met accounts for the heat storage as opposed to the two-node model used in the Conduction Transfer Function by EnergyPlus. Moreover, further interventions have to be done to allow the user to control the algorithms meant to calculate the heat transfer processes since the user is forced to run the default EnergyPlus models. For instance, the amount of absorbed short-wave radiation by the walls was reported to be overestimated using the ASHRAE Clear Sky solar model (DoE, 2019). Also, using other conduction transfer algorithms, for instance, the Heat And Moisture Transfer algorithm would have been more accurate since it considers the heat storage within a construction material. However, this algorithm was not used in this study since it requires further interventions within the code. These variations in each model's surface energy balance necessitate validating the Ladybug-tools model against in-situ measurements within diverse climates.

Furthermore, results of this study have shown that redefining the reflected radiation in terms of the direct normal radiation and weighting the surfaces' long-wave radiation by their view factors were the most effective with the largest *MRT* differences between the original and the new Ladybug-tools model in Cairo 7th June (14.8°C), particularly in N-S canyons, followed by London 19th August (13.2°C) in E-W canyons and Cairo 17th January

(6.7°C) outside the canyon. The new model showed less improvement during the daytime in London 14th February than the other scenarios. Nevertheless, further improvements could be noticed over the average layout. Also, robustness of the weather files used in the simulations has to be considered to ensure the rigor of the results acquired. Further, care has to be taken if the solar time is incident at either the simulation time or the representative date in the weather file, in order to avoid parsing data pertained to succeeding or preceding hours. Over and above, further improvements could be achieved by estimating the sky temperature in terms of the sky emissivity with reference to the cloud cover and/or the atmospheric water vapour pressure, which shall be the focus of the future work.

References

- Allegrini, J., Dorer, V. and Carmeliet, J. (2015). Influence of morphologies on the microclimate in urban neighbourhoods. Journal of Wind Engineering and Industrial Aerodynamics, 144, pp.108-117.
- Arens, E., Hoyt, T., Zhou, X., Huang, L., Zhang, H. and Schiavon, S. (2015). Modeling the comfort effects of short-wave solar radiation indoors. Building and Environment, 88, pp.3-9.
- ASHRAE (2017a). ANSI/ASHRAE Standard 55-2017: Thermal environmental conditions for human occupancy: American Society of Heating, Refrigerating and Air-Conditioning Engineers.
- ASHRAE (2017b). ASHRAE HandBook of Fundamentals (SI Edition). Atlanta: American Society of Heating, refrigerating, and Air-Conditioning Engineers Inc.
- Blazejczyk, K. (2005). MENEX_2005. The Updated Version of Man-Environment Heat Exchange Model: 14
- Bruse, M. (2020). ENVI-met. Accessed: 03/30/2020, Available at: https://www.envi-met.com/.
- DoE. (2020). Weather Data. Accessed: 20/09/2019, 2019, Available at: https://energyplus.net/weather.
- DoE, U. D. o. E. (2019). Engineering reference. EnergyPlus version 9.2.0: 58-167.
- Elnabawi, M. H., Hamza, N. and Dudek, S. (2013). Use and evaluation of the ENVI-met model for two different urban forms in Cairo, Egypt: measurements and model simulations. In: 13th Conference of International Building Performance Simulation Association, Chambéry, France.
- Engineering-ToolBox. (2001). Engineering ToolBox. Accessed: 20/09/2019, 2019, Available at: https://www.engineeringtoolbox.com/.
- Fanger, P. O. (1972). Thermal comfort; Analysis and applications in environmental engineering. NewYork: McGraw-Hill, first published in 1970, Danish Technical Press, Copenhagen.

- Forouzandeh, A. (2018). Numerical modeling validation for the microclimate thermal condition of semiclosed courtyard spaces between buildings. Sustainable Cities and Society, 36, pp.327-345.
- Huang, J., Cedeno-Laurent, J. G. and Spengler, J. D. (2014). CityComfort+: A simulation-based method for predicting mean radiant temperature in dense urban areas. Building and Environment, 80, pp.84-95.
- Huttner, S. (2012). Further development and application of the 3D microclimate simulation ENVI-met. PhD, Mainz University, Germany.
- Jamei, E. and Rajagopalan, P. (2019). Effect of street design on pedestrian thermal comfort. Architectural Science Review, 62(2), pp.92-111.
- Lindberg, F., Onomura, S. and Grimmond, C. (2016). Influence of ground surface characteristics on the mean radiant temperature in urban areas. International journal of biometeorology, 60(9), pp.1439-1452.
- Mackey, C., Galanos, T., Norford, L., Roudsari, M. S. and Architects, P. (2017). Wind, sun, surface temperature, and heat island: critical variables for high-resolution outdoor thermal comfort. In: Proceedings of the 15th International conference of Building Performance Simulation Association. San Francisco, USA.
- Matzarakis, A., Rutz, F. and Mayer, H. (2007). Modelling radiation fluxes in simple and complex environments—application of the RayMan model. International journal of biometeorology, 51(4), pp.323-334.
- McNeel, R. (2020). Rhinoceros 3D. Accessed: 03/30/2020, Available at: https://www.rhino3d.com/.
- Naboni, E., Coccolo, S., Meloni, M. and Scartezzini, J.-L. (2018). Outdoor comfort simulation of complex architectural designs: a review of simulation tools from the designer perspective. In: 2018 Building Performance Analysis Conference and SimBuild coorganized by ASHRAE and IBPSA-USA, Chicago.
- Naboni, E., Meloni, M., Coccolo, S., Kaempf, J. and Scartezzini, J.-L. (2017). An overview of simulation tools for predicting the mean radiant temperature in an outdoor space. Energy Procedia, 122, pp.1111-1116.
- Rakha, T., Zhand, P. and Reinhart, C. (2017). A Framework for Outdoor Mean Radiant Temperature Simulation: Towards Spatially Resolved Thermal Comfort Mapping in Urban Spaces. Proceedings of the 15th IBPSA, pp.2414-2420.
- Robinson, D., Haldi, F., Leroux, P., Perez, D., Rasheed, A. and Wilke, U. (2009). CitySim: Comprehensive micro-simulation of resource flows for sustainable urban planning. In: Proceedings of the Eleventh International IBPSA Conference.

- Santamouris, M., Haddad, S., Saliari, M., Vasilakopoulou, K., Synnefa, A., Paolini, R., Ulpiani, G., Garshasbi, S. and Fiorito, F. (2018). On the energy impact of urban heat island in Sydney: Climate and energy potential of mitigation technologies. Energy and Buildings, 166, pp.154-164
- Sharmin, T., Steemers, K. and Matzarakis, A. (2017). Microclimatic modelling in assessing the impact of urban geometry on urban thermal environment. Sustainable Cities and Society, 34, pp.293-308.
- Yang, X., Zhao, L., Bruse, M. and Meng, Q. (2013). Evaluation of a microclimate model for predicting the thermal behavior of different ground surfaces. Building and Environment, 60, pp.93-104.